

## Comparison of Finite Difference and Mixed Finite Element Methods for Perfectly Matched Layer Models

V. A. Bokil<sup>1,\*</sup> and M. W. Buksas<sup>2</sup>

<sup>1</sup> Department of Mathematics, Oregon State University, Corvallis, OR 97331, USA.

<sup>2</sup> CCS-4, Mail Stop D409, Los Alamos National Laboratory, NM 87544, USA.

Received 29 April 2006; Accepted (in revised version) 5 January 2007

Available online 15 February 2007

---

**Abstract.** We consider the anisotropic uniaxial formulation of the perfectly matched layer (UPML) model for Maxwell's equations in the time domain. We present and analyze a mixed finite element method for the discretization of the UPML in the time domain to simulate wave propagation on unbounded domains in two dimensions. On rectangles the spatial discretization uses bilinear finite elements for the electric field and the lowest order Raviart-Thomas divergence conforming elements for the magnetic field. We use a centered finite difference method for the time discretization. We compare the finite element technique presented to the finite difference time domain method (FDTD) via a numerical reflection coefficient analysis. We derive the numerical reflection coefficient for the case of a semi-infinite PML layer to show consistency between the numerical and continuous models, and in the case of a finite PML to study the effects of terminating the absorbing layer. Finally, we demonstrate the effectiveness of the mixed finite element scheme for the UPML by a numerical example and provide comparisons with the split field PML discretized by the FDTD method. In conclusion, we observe that the mixed finite element scheme for the UPML model has absorbing properties that are comparable to the FDTD method.

**AMS subject classifications:** 65M60, 78M10

**Key words:** Perfectly matched layers, mixed finite element methods, FDTD, Maxwell's equations.

---

## 1 Introduction

The effective modeling of electromagnetic waves on unbounded domains by numerical techniques, such as the finite difference or the finite element method, is dependent on the particular absorbing boundary condition used to truncate the computational domain. In 1994, J. P. Berenger created the *perfectly matched layer* (PML) technique for the reflectionless absorption of electromagnetic waves in the time domain [4]. The PML is

---

\*Corresponding author. *Email addresses:* bokilv@math.oregonstate.edu (V. A. Bokil), mwbuksas@lanl.gov (M. W. Buksas)

an absorbing layer that is placed around the computational domain of interest in order to attenuate outgoing radiation. Berenger showed that his PML model allowed perfect transmission of electromagnetic waves across the interface of the computational domain regardless of the frequency, polarization or angle of incidence of the waves. The waves are then attenuated exponentially with respect to depth into the absorbing layers. Since its original inception in 1994, PML's have also extended their applicability in areas other than computational electromagnetics such as acoustics, elasticity, etc., [2, 3, 15–17].

The properties of the continuous PML model have been studied extensively and are well documented. The original *split field* PML, proposed by Berenger, involved a nonphysical splitting of Maxwell's equations resulting in non-Maxwellian fields and a weakly hyperbolic system [1]. A complex change of variables approach was used in [9,20] to derive an equivalent PML model that did not require a splitting of Maxwell's equations. In [22] the authors observed that a material can possess reflectionless properties if it is assumed to be anisotropic. A single layer in this technique was termed *uniaxial*, and the PML was referred to as the uniaxial PML (UPML). In this method, modifications to Maxwell's equations are also not required and one obtains a strongly hyperbolic system. In [14,18] further study of the anisotropic PML is carried out. Unlike Berenger's split field PML, which is a nonphysical medium, the anisotropic PML can be a physically realizable medium [20]. Thus, there are several reasons for using the anisotropic PML in numerical simulations. In [24] the authors show that the anisotropic PML and Berenger's split field PML produce the same tangential fields; however, the normal fields are different as the two methods satisfy different divergence conditions.

The finite depth of the absorbing layer allows the transmitted part of the wave to return to the computational domain. In addition, the discretization of Maxwell's equations introduces errors which cause the PML to be less than perfectly matched. Even so, it has been found that the PML medium can result in reflection errors as minute as -80 dB to -100 dB [4, 5, 9, 14].

There are a number of publications that study the properties of the finite difference time domain (FDTD) method (Yee scheme [26]) for discretizing the PML model (e.g., see [23]). There are significantly fewer publications that study the properties of the finite element method for the approximation of the PML equations. A comparison of the anisotropic PML to the split field PML of Berenger was performed in [24], in which the authors implement the anisotropic PML into an edge based finite element method for a second order formulation of Maxwell's equations. In [25] the authors use the lowest order as well as first order tangential vector finite element methods for the discretization of the electric field. They compare the performance of these elements with the FDTD method when a PML is used to terminate the computational domain. They show that the lowest order elements do not perform as well as the FDTD method; however, the first order elements can produce more accurate results than FDTD. A time domain mixed finite element method has been used in [11] along with mass lumping techniques to solve scattering problems on domains where a PML method based on the Zhao-Cangellaris's model is used to terminate the mesh [27]. The underlying partial differential equations in

the Zhao-Cangellaris's PML model are second order in time, whereas the anisotropic uniaxial model consists of a system of first order PDEs. A recent paper [19] presents a new formulation to implement the complex frequency shifted perfectly matched layer (CFS-PML) for boundary truncation in a two-dimensional vector finite element time domain method directly applied to Maxwell's equations.

In this paper, we present a mixed finite element method (FEM) for the discretization of the anisotropic uniaxial formulation of the PML, by Sacks et al., [22] in the time domain to simulate electromagnetic wave propagation on unbounded regions. We divide the computational domain into rectangles. On each rectangle, we use continuous (piecewise) bilinear finite elements to discretize the electric field and the Raviart-Thomas elements [21] to discretize the magnetic field. The degrees of freedom are staggered in space as in the FDTD scheme. We use a centered finite difference scheme in time and we stagger the temporal components of the electric and magnetic fields. We study the effectiveness of the PML technique as an absorbing boundary condition for the mixed FEM by performing a numerical reflection coefficient analysis. We provide comparisons of the numerical approximations of the PML model by the mixed FEM with those of the Zhao-Cangellaris's PML model discretized using the FDTD scheme, presented in [12]. We compare simulations performed using the UPML discretized by the mixed FEM with the split field PML of Berenger discretized by the FDTD method [4]. These comparisons demonstrate that the PML technique is an effective absorbing boundary condition for the mixed FEM, which has comparable (with FDTD) absorbing properties. We have used this method in problems of scattering type in [7]. A mixed FEM was used for the discretization of a similar UPML formulation for the wave equation written as a system of first order PDE's in [8]. An advantage of FEM's is that they can model arbitrary complex geometrical structures effectively, whereas the FDTD method employs a stair stepping approach that can be very inaccurate.

An outline of the remainder of this paper is as follows. In Sections 2 and 3, we describe the UPML model and its implementation. In Section 4, we derive the two-dimensional (2D) transverse magnetic (TM) mode of the UPML model, and we describe a mixed finite element formulation for the UPML. Section 5 describes the numerical discretization in space and time. We perform a numerical reflection coefficient analysis in Section 6. In this analysis, we provide a comparison of the absorbing properties of the discrete PML model using the mixed finite element method with those using the FDTD method. Finally, we present numerical examples in Section 7 that demonstrate the effectiveness of the discrete PML model using the mixed FEM. We also compare these numerical results with those of the split field method of Berenger discretized by the FDTD method.

## 2 An anisotropic perfectly matched layer model

In this section we summarize the construction of the anisotropic PML. We refer the reader to [6] for a detailed derivation of the PML model.

We consider the time-harmonic form of Maxwell's equations with time dependence  $e^{i\omega t}$  given by

$$i\omega\hat{\mathbf{B}} = -\nabla \times \hat{\mathbf{E}}, \quad i\omega\hat{\mathbf{D}} = \nabla \times \hat{\mathbf{H}}, \quad (2.1)$$

along with zero divergence conditions on  $\hat{\mathbf{B}}$  and  $\hat{\mathbf{D}}$ . For every field vector  $\mathbf{V}$ ,  $\hat{\mathbf{V}}$  denotes its Fourier transform. Constitutive relations, which relate the electric and magnetic fluxes ( $\hat{\mathbf{D}}, \hat{\mathbf{B}}$ ) to the electric and magnetic fields ( $\hat{\mathbf{E}}, \hat{\mathbf{H}}$ ), are added to these equations to make the system fully determined and to describe the response of a material to the electromagnetic fields. The most general form of these constitutive laws are

$$\hat{\mathbf{B}} = [\hat{\mu}]\hat{\mathbf{H}}; \quad \hat{\mathbf{D}} = [\hat{\epsilon}]\hat{\mathbf{E}}, \quad (2.2)$$

where, in (2.2) the square brackets indicate a tensor quantity. The tensors  $[\hat{\epsilon}]$  and  $[\hat{\mu}]$  are defined as

$$[\hat{\epsilon}] = [\epsilon] + \frac{[\sigma_E]}{i\omega}, \quad [\hat{\mu}] = [\mu] + \frac{[\sigma_M]}{i\omega}, \quad (2.3)$$

where,  $[\epsilon]$ , and  $[\mu]$ , are the electric permittivity and the magnetic permeability tensors, respectively. Also,  $[\sigma_E]$ , and  $[\sigma_M]$ , are the electric and magnetic conductivity tensors, respectively.

The split-field PML, introduced by Berenger [4], is a hypothetical medium based on a mathematical model. In [18] Mittra and Pekel showed that Berenger's PML is equivalent to Maxwell's equations with a diagonally anisotropic tensor appearing in the constitutive relations for  $\mathbf{D}$  and  $\mathbf{B}$ . For a single interface the anisotropic medium is *uniaxial* and is composed of both the electric permittivity and magnetic permeability tensors. This uniaxial formulation performs as well as the original split-field PML while avoiding the nonphysical field splitting. By properly defining a general constitutive tensor  $[S]$ , which we will define in Section 3, we can use the UPML in the interior working volume as well as the absorbing layer. This tensor provides a lossless isotropic medium in the primary computation zone and individual UPML absorbers adjacent to the outer lattice boundary planes for mitigation of spurious wave reflections. The fields excited within the UPML are also plane wave in nature and satisfy Maxwell's curl equations.

The derivation of the PML properties for the tensor constitutive laws is done directly by Sacks et al., [22] and also by Gedney [14]. In the PML layers the impedance matching assumption must be satisfied, i.e., the impedance of the layer must match that of free space:  $\epsilon_0^{-1}\mu_0 = [\hat{\epsilon}]^{-1}[\hat{\mu}]$ . This implies

$$\frac{[\hat{\epsilon}]}{\epsilon_0} = \frac{[\hat{\mu}]}{\mu_0} = [S]. \quad (2.4)$$

Hence, the constitutive parameters inside the PML layer are  $[\hat{\epsilon}] = \epsilon_0[S]$  and  $[\hat{\mu}] = \mu_0[S]$ , where  $[S]$  is a diagonal tensor.

### 3 Implementation of the uniaxial PML

To apply the perfectly matched layer to electromagnetic computations, the half infinite layer is replaced with a layer of finite depth and backed with a more conventional boundary condition, such as a perfect electric conductor (PEC). This truncation of the layer will lead to reflections generated at the PEC surface which can propagate back through the layer to re-enter the computational region. In this case, the reflection coefficient  $R$  is a function of the angle of incidence  $\theta$ , the depth of the PML  $\delta$ , as well as the diagonal elements of the (diagonal) tensor  $[S]$  in (2.4). These diagonal elements of  $[S]$  in the PML are chosen in order for the attenuation of waves in the PML to be sufficient so that the waves striking the PEC surface are negligible in magnitude. Perfectly matched layers are then placed near each edge (face in 3D) of the computational domain where a non-reflecting condition is desired. This leads to overlapping PML regions in the corners of the domain.

As shown in [22], the correct form of the tensor which appears in the constitutive laws for these regions is the product

$$[S] = [S]_x [S]_y [S]_z, \quad (3.1)$$

where component  $[S]_\alpha$  in the product in (3.1) is responsible for attenuation in the  $\alpha$  direction, for  $\alpha = x, y, z$ . All three of the component tensors in (3.1) are diagonal and have the forms

$$[S]_x = \begin{bmatrix} s_x^{-1} & 0 & 0 \\ 0 & s_x & 0 \\ 0 & 0 & s_x \end{bmatrix}; \quad [S]_y = \begin{bmatrix} s_y & 0 & 0 \\ 0 & s_y^{-1} & 0 \\ 0 & 0 & s_y \end{bmatrix}; \quad [S]_z = \begin{bmatrix} s_z & 0 & 0 \\ 0 & s_z & 0 \\ 0 & 0 & s_z^{-1} \end{bmatrix}. \quad (3.2)$$

Here  $s_\alpha$  governs the attenuation of the electromagnetic waves in the  $\alpha$  direction for  $\alpha = x, y, z$ .

When designing PMLs for implementation, it is important to choose the parameters  $s_\alpha$  so that the resulting frequency domain equations can be easily converted back into the time domain. The simplest of these [14] which we employ here is

$$s_\alpha = 1 + \frac{\sigma_\alpha}{i\omega\epsilon_0}, \quad \text{where } \sigma_\alpha \geq 0, \quad \alpha = x, y, z. \quad (3.3)$$

The PML interface represents a discontinuity in the conductivities  $\sigma_\alpha$ . To reduce the numerical reflections caused by these discontinuous conductivities the  $\sigma_\alpha$  are chosen to be functions of the variable  $\alpha$  (for e.g.,  $\sigma_x$  is taken to be a function of  $x$  in the  $[S]_x$  component of the PML tensor). Choosing these functions so that  $\sigma_\alpha = 0$ , i.e.,  $s_\alpha = 1$ , at the interface makes the PML a continuous extension of the medium being matched and reduces numerical reflections at the interface. Increasing the value of  $\sigma_\alpha$  with depth in the layer allows for greater overall attenuation while keeping down the numerical reflections. Gedney [14] suggests a conductivity profile

$$\sigma_\alpha(\alpha) = \frac{\sigma_{\max} |\alpha - \alpha_0|^m}{\delta^m}, \quad \alpha = x, y, z, \quad (3.4)$$

where  $\delta$  is the depth of the layer,  $\alpha = \alpha_0$  is the interface between the PML and the computational domain, and  $m$  is the order of the polynomial variation. Gedney remarks that values of  $m$  between 3 and 4 are believed to be optimal. For the conductivity profile (3.4) the PML parameters can be determined for given values of  $m, \delta$ , and the desired reflection coefficient at normal incidence,  $R_0$ , as

$$\sigma_{\max} \approx \frac{(m+1)\ln(1/R_0)}{2\delta}. \quad (3.5)$$

#### 4 A mixed finite element formulation for the UPML in two dimensions

From the time-harmonic Maxwell's curl equations in the UPML (2.1) along with (2.2), (2.3) and (2.4), Ampere's and Faraday's laws can be written as

$$\begin{cases} i\omega\mu_0[S]\hat{\mathbf{H}} = -\nabla \times \hat{\mathbf{E}} & \text{(Maxwell-Faraday's Law),} \\ i\omega\epsilon_0[S]\hat{\mathbf{E}} = \nabla \times \hat{\mathbf{H}} & \text{(Maxwell-Ampere's Law).} \end{cases} \quad (4.1)$$

In (4.1),  $[S]$  is the diagonal tensor defined via (3.1)-(3.5). In the presence of this diagonal tensor a plane wave is purely transmitted into the uniaxial medium. The tensor  $[S]$  is no longer uniaxial by strict definition but rather is anisotropic. However, the anisotropic PML is still referred to as uniaxial, since it is uniaxial in the non overlapping PML regions.

Let  $\partial_q = \partial/\partial q$  denote the derivative w.r.t  $q$ , for  $q = x, y, z, t$ . To obtain the 2D model of the UPML we assume no variation in the  $z$  direction (i.e.,  $\partial_z = 0$ ). In the 2D transverse magnetic (TM) mode the electromagnetic field has three components  $E_z$ ,  $H_x$ , and  $H_y$ . In this case, we have  $\sigma_z = 0$  and  $s_z = 1$  in the UPML, and the time-harmonic Maxwell's equations (4.1) in the uniaxial medium can be written in scalar form as

$$\begin{cases} i\omega\mu_0s_ys_x^{-1}\hat{H}_x = -\partial_y\hat{E}_z, \\ i\omega\mu_0s_xs_y^{-1}\hat{H}_y = -\partial_x\hat{E}_z, \\ i\omega\epsilon_0s_xs_y\hat{E}_z = \partial_x\hat{H}_y - \partial_y\hat{H}_x. \end{cases} \quad (4.2)$$

To avoid a computationally intensive implementation we define suitable constitutive relationships that facilitate the decoupling of the frequency dependent terms [23]. To this end, we introduce the fields

$$\begin{cases} \hat{B}_x = \mu_0s_x^{-1}\hat{H}_x, \\ \hat{B}_y = \mu_0s_y^{-1}\hat{H}_y, \\ \hat{D}_z = \mu_0s_y\hat{E}_z. \end{cases} \quad (4.3)$$

Substituting the definitions (4.3) in (4.2), using the defining relations for  $s_x$  and  $s_y$  from (3.3), and then transforming into the time domain by using the inverse Fourier transform

yields an equivalent system of time-domain differential equations given as

$$\begin{cases} \partial_t \mathbf{B} = -\frac{1}{\epsilon_0} \Sigma_2 \mathbf{B} - \overrightarrow{\text{curl}} E, \\ \partial_t \mathbf{H} = \frac{1}{\mu_0} \partial_t \mathbf{B} + \frac{1}{\epsilon_0 \mu_0} \Sigma_1 \mathbf{B}, \\ \partial_t D = -\frac{1}{\epsilon_0} \sigma_x D + \text{curl} \mathbf{H}, \\ \partial_t E = -\frac{1}{\epsilon_0} \sigma_y E + \frac{1}{\epsilon_0} \partial_t D. \end{cases} \quad (4.4)$$

In the above  $\mathbf{H} = (H_x, H_y)^T$ ,  $\mathbf{B} = (B_x, B_y)^T$ ,  $E = E_z$  and  $D = D_z$ . Also, in (4.4)

$$\Sigma_1 = \begin{pmatrix} \sigma_x & 0 \\ 0 & \sigma_y \end{pmatrix}; \quad \Sigma_2 = \begin{pmatrix} \sigma_y & 0 \\ 0 & \sigma_x \end{pmatrix}. \quad (4.5)$$

Let  $\mathbb{D}$  denote the computational domain in  $\mathbb{R}^2$ . We denote the domain  $\mathbb{D}$  along with the surrounding finite PML layers by  $\Omega$ . In (4.4), the operators denoted by  $\overrightarrow{\text{curl}}$ , and  $\text{curl}$  are linear differential operators which are defined as

$$\overrightarrow{\text{curl}} \phi = (\partial_y \phi, -\partial_x \phi)^T, \quad \forall \phi \in \mathcal{D}'(\Omega), \quad (4.6)$$

$$\text{curl} \mathbf{v} = \partial_x v_y - \partial_y v_x, \quad \forall \mathbf{v} = (v_x, v_y)^T \in \mathcal{D}'(\Omega)^2, \quad (4.7)$$

where  $\mathcal{D}'(\Omega)$  is the space of distributions on  $\Omega$ . The operator  $\text{curl}$  appears as the (formal) transpose of the operator  $\overrightarrow{\text{curl}}$  [13], i.e.,

$$\langle \text{curl} \mathbf{v}, \phi \rangle = \langle \mathbf{v}, \overrightarrow{\text{curl}} \phi \rangle, \quad \forall \mathbf{v} \in \mathcal{D}'(\Omega)^2, \phi \in \mathcal{D}'(\Omega), \quad (4.8)$$

with  $\langle \cdot, \cdot \rangle$  being the appropriate inner product. Thus, the PML model consists in solving system (4.4) for the six variables  $B_x, B_y, H_x, H_y, D, E$  in  $\Omega$ , with PEC conditions on  $\partial\Omega$  to terminate the PML; namely,  $\mathbf{n} \times \mathbf{E} = 0$ , on  $\partial\Omega$ , where  $\mathbf{n}$  is the outward unit normal to  $\partial\Omega$ . In the case of the 2D TM mode the PEC condition translates to  $E = E_z = 0$ , on  $\partial\Omega$ .

Based on the above discussion, we consider the following variational formulation of system (4.4) which is suitable for discretization by finite elements.

Find  $(E(\cdot, t), D(\cdot, t), \mathbf{H}(\cdot, t), \mathbf{B}(\cdot, t)) \in H_0^1(\Omega) \times H_0^1(\Omega) \times [L^2(\Omega)]^2 \times [L^2(\Omega)]^2$  such that for all  $\Psi \in [L^2(\Omega)]^2$ , for all  $\phi \in H_0^1(\Omega)$ ,

$$\begin{cases} \frac{d}{dt} \int_{\Omega} \mathbf{B} \cdot \Psi \, d\mathbf{x} = -\frac{1}{\epsilon_0} \int_{\Omega} \Sigma_2 \mathbf{B} \cdot \Psi \, d\mathbf{x} - \int_{\Omega} \overrightarrow{\text{curl}} E \cdot \Psi \, d\mathbf{x}, \\ \frac{d}{dt} \int_{\Omega} \mathbf{H} \cdot \Psi \, d\mathbf{x} = \frac{1}{\mu_0} \frac{d}{dt} \int_{\Omega} \mathbf{B} \cdot \Psi \, d\mathbf{x} + \frac{1}{\epsilon_0 \mu_0} \int_{\Omega} \Sigma_1 \mathbf{B} \cdot \Psi \, d\mathbf{x}, \\ \frac{d}{dt} \int_{\Omega} D \cdot \phi \, d\mathbf{x} = -\frac{1}{\epsilon_0} \int_{\Omega} \sigma_x D \cdot \phi \, d\mathbf{x} + \int_{\Omega} \overrightarrow{\text{curl}} \phi \cdot \mathbf{H} \, d\mathbf{x}, \\ \frac{d}{dt} \int_{\Omega} E \cdot \phi \, d\mathbf{x} = -\frac{1}{\epsilon_0} \int_{\Omega} \sigma_y E \cdot \phi \, d\mathbf{x} + \frac{1}{\epsilon_0} \frac{d}{dt} \int_{\Omega} D \cdot \phi \, d\mathbf{x}, \end{cases} \quad (4.9)$$

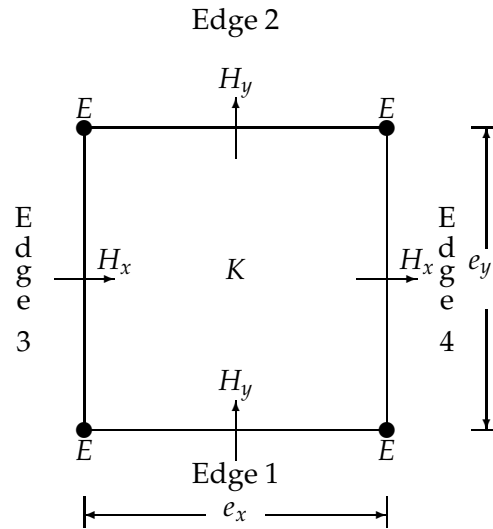


Figure 1: A sample domain element  $K$ . The degrees of freedom for the electric and magnetic fields are staggered in space. The degrees of freedom for the electric field  $E$  are at the nodes of the square. The degrees of freedom for  $H_x$  and  $H_y$  are at the midpoints of edges parallel to the  $x$ -axis and  $y$ -axis, respectively.

along with the initial conditions

$$E(x,0) = E_0, \quad D(x,0) = D_0, \quad \mathbf{H}(x,0) = \mathbf{H}_0, \quad \mathbf{B}(x,0) = \mathbf{B}_0, \quad \text{for } x \in \Omega. \quad (4.10)$$

We assume that the fields  $(E, D, \mathbf{H}, \mathbf{B})$  are sufficiently differentiable in time. We note that, for  $E \in L^2(\Omega)$ ,  $\overrightarrow{\text{curl}} E = (\partial_y E, -\partial_x E)^T \in [L^2(\Omega)]^2$  implies that both the partial derivatives of  $E$  must be in  $L^2(\Omega)$ . Hence we must have  $E \in H^1(\Omega)$ .

In [6] we have derived energy decay results for the 2D TM mode of the UPML (4.9), for specific values of  $\sigma_x$  and  $\sigma_y$ .

## 5 The discrete mixed finite element scheme

### 5.1 Spatial discretization

Let  $\Omega$  be a union of rectangles defining a regular mesh  $(\mathcal{T}_h)$  with square elements  $(K)$  of edge  $h > 0$  as in Fig. 1. We consider the following approximation space for  $\mathbf{H}$  and  $\mathbf{B}$ :

$$\mathcal{V}_h = \left\{ \Psi_h \in [L^2(\Omega)]^2 \mid \forall K \in \mathcal{T}_h, \Psi_h|_K \in RT_{[0]} \right\}, \quad (5.1)$$

where,  $RT_{[0]} = P_{10} \times P_{01}$ , is the lowest order Raviart-Thomas space [21] and for  $k_1, k_2 \in \mathbb{N} \cup \{0\}$ ,

$$P_{k_1 k_2} = \left\{ p(x_1, x_2) \mid p(x_1, x_2) = \sum_{0 \leq i \leq k_1} \sum_{0 \leq j \leq k_2} a_{ij} x_1^i x_2^j \right\}.$$

The basis functions for  $H_x$  have unity value along an  $e_y$  edge and are zero over all other edges. Similarly, the basis functions for  $H_y$  have unity value along an  $e_x$  edge and are zero over all other edges (see Fig. 1).

The approximation space for  $E$  and  $D$  is chosen to be

$$\mathcal{U}_h = \{\phi_h \in H_0^1(\Omega) \mid \forall K \in \mathcal{T}_h, \phi_h|_K \in Q_1\}, \tag{5.2}$$

where the space  $Q_1 = P_{11}$ . The basis functions for  $E$  have unity value at one node and are zero at all other nodes. Fig. 1 shows the locations for the degrees of freedom for the electric and magnetic fields.

Based on the approximation spaces described above the spatially discrete scheme is: Find  $(E_h(\cdot, t), D_h(\cdot, t), \mathbf{H}_h(\cdot, t), \mathbf{B}_h(\cdot, t)) \in \mathcal{U}_h \times \mathcal{U}_h \times \mathcal{V}_h \times \mathcal{V}_h$  such that for all  $\Psi_h \in \mathcal{V}_h$ , and for all  $\phi_h \in \mathcal{U}_h$ ,

$$\begin{cases} \frac{d}{dt} \int_{\Omega} \mathbf{B}_h \cdot \Psi_h d\mathbf{x} = -\frac{1}{\epsilon_0} \int_{\Omega} \Sigma_1 \mathbf{B}_h \cdot \Psi_h d\mathbf{x} - \int_{\Omega} \overrightarrow{\text{curl}} E_h \cdot \Psi_h d\mathbf{x}, \\ \frac{d}{dt} \int_{\Omega} \mathbf{H}_h \cdot \Psi_h d\mathbf{x} = \frac{1}{\mu_0} \frac{d}{dt} \int_{\Omega} \mathbf{B}_h \cdot \Psi_h d\mathbf{x} + \frac{1}{\epsilon_0 \mu_0} \int_{\Omega} \Sigma_2 \mathbf{B}_h \cdot \Psi_h d\mathbf{x}, \\ \frac{d}{dt} \int_{\Omega} D_h \cdot \phi_h d\mathbf{x} = -\frac{1}{\epsilon_0} \int_{\Omega} \sigma_x D_h \cdot \phi_h d\mathbf{x} + \int_{\Omega} \overrightarrow{\text{curl}} \phi_h \cdot \mathbf{H}_h d\mathbf{x}, \\ \frac{d}{dt} \int_{\Omega} E_h \cdot \phi_h d\mathbf{x} = -\frac{1}{\epsilon_0} \int_{\Omega} \sigma_y E_h \cdot \phi_h d\mathbf{x} + \frac{1}{\epsilon_0} \frac{d}{dt} \int_{\Omega} D_h \cdot \phi_h d\mathbf{x}. \end{cases} \tag{5.3}$$

### 5.2 Temporal discretization

For the temporal discretization we use a centered second order accurate finite difference scheme. For  $k \in \mathbb{Z}$  let,

$$D_{\Delta t} V^k = \frac{V^{k+1/2} - V^{k-1/2}}{\Delta t}, \quad \overline{V}^k = \frac{V^{k+1/2} + V^{k-1/2}}{2}. \tag{5.4}$$

Let  $(\cdot, \cdot)$  denote the inner product in  $L^2(\Omega)$ . We can now describe the fully discrete scheme in space and time as: Find  $(E_h^{n+1}, D_h^{n+1}, \mathbf{H}_h^{n+\frac{1}{2}}, \mathbf{B}_h^{n+\frac{1}{2}}) \in \mathcal{U}_h \times \mathcal{U}_h \times \mathcal{V}_h \times \mathcal{V}_h$  such that for all  $\Psi_h \in \mathcal{V}_h$ , for all  $\phi_h \in \mathcal{U}_h$ ,

$$\begin{cases} \text{(i)} & (D_{\Delta t} \mathbf{B}_h^n, \Psi_h) = -\frac{1}{\epsilon_0} (\Sigma_2 \overline{\mathbf{B}}_h^n, \Psi_h) - (\overrightarrow{\text{curl}} E_h^n, \Psi_h), \\ \text{(ii)} & (D_{\Delta t} \mathbf{H}_h^n, \Psi_h) = \frac{1}{\mu_0} (D_{\Delta t} \mathbf{B}_h^n, \Psi_h) + \frac{1}{\epsilon_0 \mu_0} (\Sigma_1 \overline{\mathbf{B}}_h^n, \Psi_h), \\ \text{(iii)} & (D_{\Delta t} D_h^{n+\frac{1}{2}}, \phi_h) = -\frac{1}{\epsilon_0} (\sigma_x \overline{D}_h^{n+\frac{1}{2}}, \phi_h) + (\overrightarrow{\text{curl}} \phi_h, \mathbf{H}_h^{n+\frac{1}{2}}), \\ \text{(iv)} & (D_{\Delta t} E_h^{n+\frac{1}{2}}, \phi_h) = -\frac{1}{\epsilon_0} (\sigma_y \overline{E}_h^{n+\frac{1}{2}}, \phi_h) + \frac{1}{\epsilon_0} (D_{\Delta t} D_h^{n+\frac{1}{2}}, \phi_h). \end{cases} \tag{5.5}$$

## 6 Analysis of the discrete PML model

In this section we study the properties of the discrete mixed FEM-UPML model by performing a plane wave analysis to calculate the reflection coefficient. We refer the reader to [6] for a detailed stability and dispersion analysis of the mixed FEM method for the discretization of the UPML and a comparison with the FDTD scheme.

In the discrete setting the PML model is no longer perfectly matched since the discretization introduces some error which manifests itself as spurious reflections. There is also error that is introduced due to the termination of the PML. We study the errors introduced in the discrete model by calculating the reflection coefficient of an infinite PML (to study the errors caused by the discretization) as well as the reflection coefficient of a finite PML (to study the errors introduced by terminating the PML).

For simplicity we assume in this section that  $\epsilon_0 = \mu_0 = 1$ . Let us also assume an infinite PML in the region  $x > 0$ . Thus,  $\sigma_y = 0$  and let  $\sigma_x = \sigma$ . Considering exact integration in time, we will look for solutions of the form

$$V(x, y, t) = \hat{V}(x, y) e^{i\omega t}, \tag{6.1}$$

to the semi-discrete system (5.3). Substituting (6.1) in (5.3), we obtain the time harmonic system

$$\begin{cases} i\omega(\hat{B}_x, \psi_x) = -(\partial_y \hat{E}, \psi_x), \\ i\omega(\hat{H}_x, \psi_x) = i\omega \left( \left(1 + \frac{\sigma}{i\omega}\right) \hat{B}_x, \psi_x \right), \\ i\omega \left( \left(1 + \frac{\sigma}{i\omega}\right) \hat{B}_y, \psi_y \right) = (\partial_x \hat{E}, \psi_y), \\ i\omega(\hat{H}_y, \psi_y) = i\omega(\hat{B}_y, \psi_y), \\ i\omega \left( \left(1 + \frac{\sigma}{i\omega}\right) \hat{D}, \phi \right) = (\hat{H}_x, \partial_y \phi) - (\hat{H}_y, \partial_x \phi), \\ i\omega(\hat{E}, \phi) = i\omega(\hat{D}, \phi). \end{cases} \tag{6.2}$$

We assume that  $\sigma$  is a piecewise constant function of  $x$  with jumps at  $x = lh, l = 0, 1, 2, \dots$ , where  $h = h_x = h_y$  is the mesh step size. Let

$$\sigma_l = \begin{cases} \text{Value of } \sigma \text{ on } (lh, (l+1)h), & \text{if } l \geq 0, \\ 0, & \text{if } l < 0. \end{cases} \tag{6.3}$$

Using the definition (3.3), we have

$$s_{x,l} = s_l = 1 + \frac{\sigma_l}{i\omega}. \tag{6.4}$$

Since  $\sigma_y = 0$ , we have  $s_y = 1$ . The PML is in the half space  $x > 0$  and the computational domain is in the half space  $x < 0$ . Therefore,  $x = 0$  is the interface between the PML and

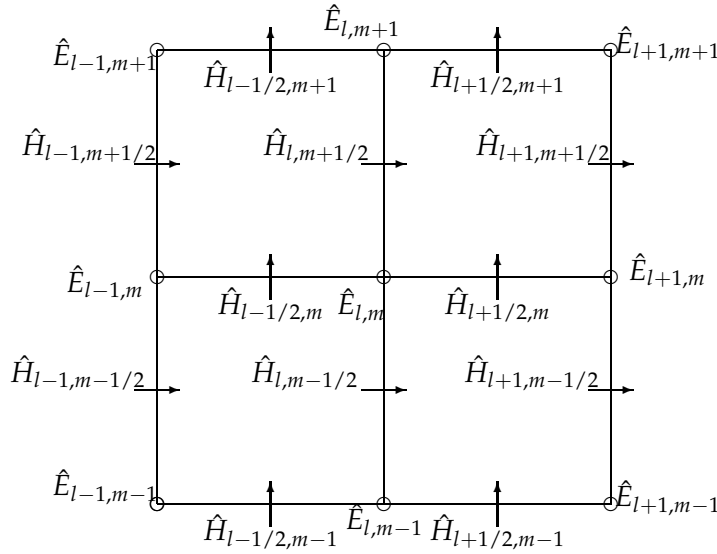


Figure 2: Dependency diagram for an interior super element.

the interior computational region. Let us define the following matrix vector products for an arbitrary double subscripted vector  $u$ :

$$\begin{cases} M_x u_{l,m} = 4u_{l,m} + u_{l-1,m} + u_{l+1,m}, \\ M_y u_{l,m} = 4u_{l,m} + u_{l,m-1} + u_{l,m+1}, \\ \tilde{S}_x u_{l,m} = M_y u_{l-1/2,m} - M_y u_{l+1/2,m}, \\ \tilde{S}_y u_{l,m} = M_x u_{l,m-1/2} - M_x u_{l,m+1/2}, \\ M_z u_{l,m} = M_x M_y u_{l,m}. \end{cases} \quad (6.5)$$

Consider an interior super element as shown in Fig. 2. Using the definitions from (6.5) in the spatial discretization of (6.2), we obtain the following system of equations that corresponds to the spatially discrete mixed finite element scheme (5.3):

$$\begin{cases} M_x \hat{B}_{l,m+1/2} = \frac{i}{\omega h} M_x (\hat{E}_{l,m+1} - \hat{E}_{l,m}), \\ M_x \hat{H}_{l,m+1/2} = \left( \frac{s_l + s_{l-1}}{2} \right) M_x \hat{B}_{l,m+1/2}, \\ s_l M_y \hat{B}_{l+1/2,m} = \frac{-i}{\omega h} M_y (\hat{E}_{l+1,m} - \hat{E}_{l,m}), \\ M_y \hat{H}_{l+1/2,m} = M_y \hat{B}_{l+1/2,m}, \\ \left( \frac{s_l + s_{l-1}}{2} \right) M_z \hat{D}_{l,m} = \frac{-6i}{\omega h} (\tilde{S}_y \hat{H}_{l,m} - \tilde{S}_x \hat{H}_{l,m}), \\ M_z \hat{E}_{l,m} = M_z \hat{D}_{l,m}. \end{cases} \quad (6.6)$$

Combining the equations in (6.6), we obtain an equation in  $E$  by eliminating the other variables

$$-\frac{\omega^2 h^2}{6} \left( \frac{s_l + s_{l-1}}{2} \right) M_z \hat{E}_{l,m} = \left( \frac{s_l + s_{l-1}}{2} \right) (M_x \hat{E}_{l,m+1} - 2M_x \hat{E}_{l,m} + M_x \hat{E}_{l,m-1}) + \frac{1}{s_l} (M_y \hat{E}_{l+1,m} - M_y \hat{E}_{l,m}) - \frac{1}{s_{l-1}} (M_y \hat{E}_{l,m} - M_y \hat{E}_{l-1,m}). \quad (6.7)$$

We now look for solutions to (6.7) of the form

$$\hat{E}_{l,m} = \hat{E}_l e^{-ik_y m h}. \quad (6.8)$$

After substituting (6.8) in (6.7), and performing some algebra, we obtain

$$-\frac{\zeta \omega^2 h^2}{6} \left( \frac{s_l + s_{l-1}}{2} \right) (4\hat{E}_l + \hat{E}_{l-1} + \hat{E}_{l+1}) = \frac{1}{s_l} (\hat{E}_{l+1} - \hat{E}_l) - \frac{1}{s_{l-1}} (\hat{E}_l - \hat{E}_{l-1}), \quad (6.9)$$

where the coefficient  $\zeta$  is defined as

$$\zeta = 1 - \frac{12}{\omega^2 h^2} \left( \frac{\sin^2(k_y h/2)}{1 + 2\cos^2(k_y h/2)} \right). \quad (6.10)$$

Let  $k_x$  and  $k_x^{\text{pml}}$  be the  $x$  components of the wave vector in free space and the PML, respectively. To calculate the reflection coefficient for the infinite PML, we look for solutions to (6.9) of the form

$$\hat{E}_l = \begin{cases} e^{-ik_x h l} + R e^{ik_x h l}, & \text{for } l < 0, \\ T e^{-k_x^{\text{pml}} h l}, & \text{for } l > 0, \end{cases} \quad (6.11)$$

where the reflection coefficient is  $R$ , and  $T$  is the transmission coefficient. Consider the equations associated to the node at the interface  $l=0$  and one node each on either side of the interface at  $l=1$ , and  $l=-1$ . From (6.9) we have

$$\begin{cases} -\frac{\zeta \omega^2 h^2}{6} (4\hat{E}_{-1} + \hat{E}_{-2} + \hat{E}_0) = (\hat{E}_0 - \hat{E}_{-1}) - (\hat{E}_{-1} - \hat{E}_{-2}), \\ -\frac{\zeta \omega^2 h^2}{6} \left( \frac{1+s_0}{2} \right) (4\hat{E}_0 + \hat{E}_{-1} + \hat{E}_1) = \frac{1}{s_0} (\hat{E}_1 - \hat{E}_0) - (\hat{E}_0 - \hat{E}_{-1}), \\ -\frac{\zeta \omega^2 h^2}{6} \left( \frac{s_1+s_0}{2} \right) (4\hat{E}_1 + \hat{E}_0 + \hat{E}_2) = \frac{1}{s_1} (\hat{E}_2 - \hat{E}_1) - \frac{1}{s_0} (\hat{E}_1 - \hat{E}_0), \end{cases} \quad (6.12)$$

where  $\zeta$  is defined in (6.10), and  $s_l$  is defined in (6.4). Substituting for  $\hat{E}_l$  from (6.11) in (6.12) we obtain three equations in the unknowns  $\hat{E}_0$ ,  $R$  and  $T$ . Solving these resulting equations for  $R$ , we can show that the reflection coefficient has the Taylor series expansion

$$R = -\frac{1}{16\omega^2} (\omega^2 - k_y^2) \sigma (\sigma + 2i\omega) h^2 + \frac{1}{48\omega^3} \sigma^2 (\sigma + 2i\omega) (\omega^2 - k_y^2)^{3/2} h^3 + \mathcal{O}(h^4). \quad (6.13)$$

The formula (6.13) implies that the reflection coefficient is proportional to  $h^2$ .

Next, we study the effects of terminating the PML by a PEC. This amounts to setting  $\hat{E}=0$  at the boundary  $x=\delta=Nh$  of the PML, i.e.  $\hat{E}_N=0$ . Here,  $N$  is the number of nodes per wavelength, i.e., the thickness of the PML is one wavelength and the number of nodes per wavelength is equal to the number of nodes in the PML. To obtain the reflection coefficient we write equation (6.9) for all the nodes in the PML as well as for the node at the interface of the working volume and PML,  $\hat{E}_0$ , and node  $\hat{E}_{-1}$  in the working volume which is  $h$  distance away from the interface. Assuming that we know the value of  $\hat{E}_{-2}$  we obtain a system of equations

$$A\mathbf{E} = -(\omega^2 h^2 \zeta + 6)E_{-2}\tilde{e}_1. \tag{6.14}$$

In the above  $\mathbf{E} = [\hat{E}_{-1}, \hat{E}_0, \hat{E}_1, \dots, \hat{E}_{N-1}]^T$ ,  $\tilde{e}_1 = [1, 0, 0, \dots]^T$  and the matrix of coefficients obtained from (6.9) is

$$A = \begin{bmatrix} b_{-1} & c_0 & 0 & \dots & 0 \\ a_{-1} & b_0 & c_1 & 0 & \dots & 0 \\ 0 & a_0 & b_1 & c_2 & \ddots & \vdots \\ \vdots & \ddots & \ddots & \ddots & \ddots & 0 \\ 0 & 0 & \dots & 0 & a_{N-2} & b_{N-1} \end{bmatrix}, \tag{6.15}$$

where

$$\begin{aligned} a_l &= \zeta \omega^2 h^2 \left( \frac{s_{l+1} + s_l}{2} \right) + \frac{6}{s_l}, \\ b_l &= 4\zeta \omega^2 h^2 \left( \frac{s_{l-1} + s_l}{2} \right) - 6 \left( \frac{1}{s_l} + \frac{1}{s_{l-1}} \right), \\ c_l &= \zeta \omega^2 h^2 \left( \frac{s_{l-1} + s_{l-2}}{2} \right) + \frac{6}{s_{l-1}}. \end{aligned} \tag{6.16}$$

We can solve system (6.15) for the value of  $R$  by using (6.11) for  $l = -1$  and  $l = -2$ . In this case the reflection coefficient is calculated to be

$$R = -e^{2ik_x h} \left( \frac{1 + (\omega^2 h^2 \zeta + 6)\kappa e^{ik_x h}}{1 + (\omega^2 h^2 \zeta + 6)\kappa e^{-ik_x h}} \right), \tag{6.17}$$

where  $\kappa$  is the first diagonal entry in  $A^{-1}$ .

Fig. 3 plots the reflection coefficient in decibels, Db (i.e.,  $20\log_{10} R$ ), versus the number of nodes per wavelength  $N$  for different values of  $R_0$ , the reflection coefficient at normal incidence for  $\theta = 0$  (top) and  $\theta = \pi/4$  (bottom). Fig. 4 plots the reflection coefficient in Db versus the angle of incidence  $\theta$  for  $R_0 = 10^{-2}$  (top) and  $R_0 = 10^{-4}$  (bottom). In these figures we compare the reflection coefficient for the mixed FEM scheme with the reflection coefficient for the TE mode of the Zhao-Cangellaris's PML model using the FDTD scheme which was presented in [12]. As can be seen in these plots the reflection properties of the FEM compare well with those of the FDTD method.

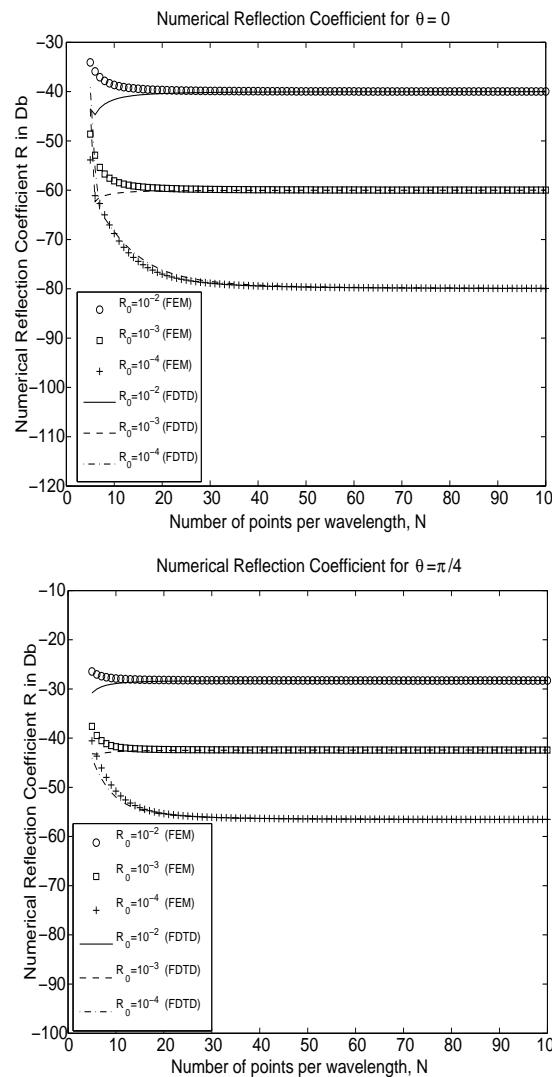


Figure 3: Numerical reflection coefficient for  $\theta=0$  (top) and  $\theta=\pi/4$  (bottom). We note that, as we increase the number of nodes per wavelength, the numerical reflection coefficient in both cases approaches  $R_0^{\cos\theta}$  (exact). In this plot  $\sigma_{\max}=3$ .

We note that the numerical reflection coefficient converges to the reflection coefficient of the continuous model, which is  $R_0^{\cos\theta}$  as we increase the value of  $N$ . We also note that as  $\theta$  approaches the value  $\pi$  the numerical reflection coefficient approaches the value 1. This is a well known behavior of PML models, i.e., waves that are propagating transversely to the interface between the domain of interest and a single PML, are not absorbed by the PML. However, these waves get absorbed into the corner regions where two PMLs overlap. We note again that the plots were obtained by considering PMLs that are one wavelength thick, i.e., the number of nodes per wavelength is the number of nodes in the

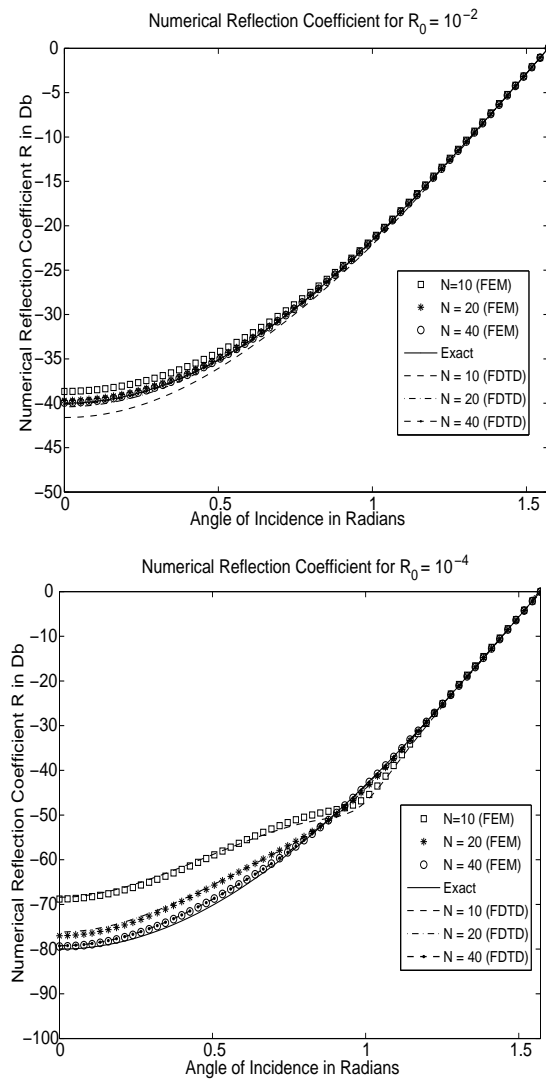


Figure 4: Numerical reflection coefficient for  $R_0 = 10^{-2}$  (top),  $R_0 = 10^{-4}$  (bottom). As  $N$  is increased, the numerical reflection coefficient converges to  $R_0^{\cos\theta}$  (exact). In this plot  $\sigma_{\max} = 3$ .

#### PML.

Fig. 5 (left) plots the convergence of the numerical reflection coefficient to the theoretical reflection coefficient, as the number of points per wavelength is increased. Here we have used  $\theta = 0$ . In all the above figures the polynomial grading (3.4) was chosen for  $\sigma$  with  $m = 3$  and  $\sigma_{\max}$  as in (3.5). The PML is in the region  $x > 0$ . Thus,  $x_0 = 0$  in (3.4) for  $\alpha = x$ .

The power of the polynomial grading for  $\sigma$  has an effect on the numerical reflection errors as is known from analysis of PML models discretized using the FDTD scheme. In

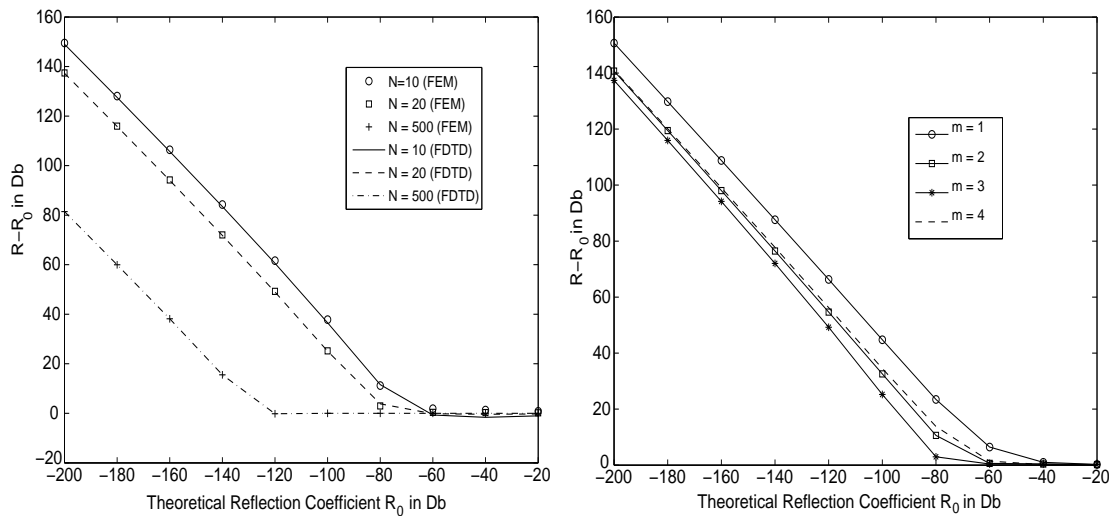


Figure 5: Difference between numerical and theoretical reflection coefficient ( $\theta = 0$ ) versus the theoretical reflection coefficient for different values of  $N$  for both the FDTD and mixed FEM methods (left), and for different values of the polynomial grading  $m$  for  $\sigma$  in the FEM method (right).

Fig. 5 (right), we plot the difference of the numerical and theoretical reflection coefficients for the mixed FEM scheme against the theoretical reflection coefficient  $R_0$  for  $m \in \{1, 2, 3, 4\}$  with  $\theta = 0$  and  $N = 20$ . This figure demonstrates the strong influence of the power  $m$  of the polynomial grading for  $\sigma$  on the reflection coefficient.

As indicated in (6.3),  $\sigma$  is a piecewise constant function of  $x$  with jumps at  $x = lh$ ,  $l = 0, 1, 2, \dots$ , where  $h$  is the mesh step size. Thus,  $\sigma_l$  is constant on the interval  $(lh, (l+1)h)$ . To generate Figs. 3, 4 and 5 we have used  $\sigma_l$  defined by (3.4) and (3.5) at  $(l+1/2)h$  as the constant value in  $(lh, (l+1)h)$  ( $s_{l+1/2}$  in Fig. 6). In Fig. 6 we plot the difference in the numerical and theoretical reflection coefficients against the theoretical reflection coefficients for different definitions of  $\sigma_l$  using  $\theta = 0$  and  $N = 20$ . The graph corresponding to  $s_0$  uses  $\sigma_l$  defined at the left endpoint i.e.,  $lh$ , as the constant value in  $(lh, (l+1)h)$ . Similarly, the graphs related to  $s_{l+1/2}$  and  $s_l$  correspond to using  $\sigma_l$  defined at  $(l+1/2)h$  and  $lh$ , respectively, as the constant value of  $\sigma_l$  in the interval  $(lh, (l+1)h)$ . As can be seen, the different choices have an effect on the numerical reflection coefficient.

## 7 Absorption of a pulse on the boundaries of a computational domain

The numerical experiment described in this section evaluates the performance of the UPML when a pulse strikes the boundaries of a computational domain. We measure the amount of reflection that an outward propagating pulse produces as it moves from free space to a boundary surrounded by absorbing PMLs.

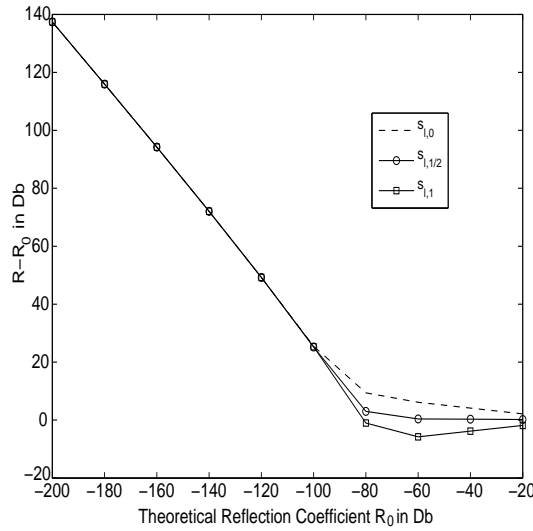


Figure 6: Difference between numerical and theoretical reflection coefficient ( $\theta = 0$ ) versus the theoretical reflection coefficient with  $N=20$  for different definitions of  $\sigma_1$  in the FEM method.

We choose our domain  $\Omega$  to be the square  $[0,12] \times [0,12]$ , with a source located at the center (6,6) of the square. The domain is surrounded by absorbing layers on all four boundaries. We discretize the problem with a rectangular grid composed of  $90 \times 90$  square elements of step size  $h = 2/15$  and the time step is  $\Delta t = 0.04/c$  (chosen to satisfy the stability condition [6]). The source is taken to be the function [10]

$$f(x,y,t) = f_1(x,y)f_2(t),$$

where

$$f_2(t) = \begin{cases} -2\pi^2 f_0^2 (t-t_0)e^{-\pi^2 f_0^2 (t-t_0)^2}, & \text{if } t \leq 2t_0, \\ 0, & \text{if } t \geq 2t_0. \end{cases} \tag{7.1}$$

In the above,  $f_0 = \frac{c}{20h}$  is the central frequency and  $t_0 = 1/f_0$ . The function  $f_1(x,y)$  is defined as

$$f_1(x,y) = e^{-7\sqrt{(x-6)^2+(y-6)^2}}. \tag{7.2}$$

We obtain a reference solution by using the mixed FEM for the TM mode of Maxwell’s equations on a larger domain  $\Omega_R$  containing  $360 \times 360$  square elements, and the same mesh step size and time step. The domain  $\Omega_R$  is terminated using PEC conditions on its boundary. We have used the polynomial grading (3.4) for  $\sigma$  with the optimal value of  $\sigma_{\max}$  as given in (3.5) with  $m = 3.5$ .

The  $L^2$  norm of the error due to numerical reflections, which arise due to the finite PML terminated by PEC conditions, is obtained by subtracting at each time step the field  $E$  at any grid point inside  $\Omega$ , from the field  $E$  at the corresponding point in  $\Omega_R$ , taking the square of this difference and summing such differences over all grid points in  $\Omega$ . We do

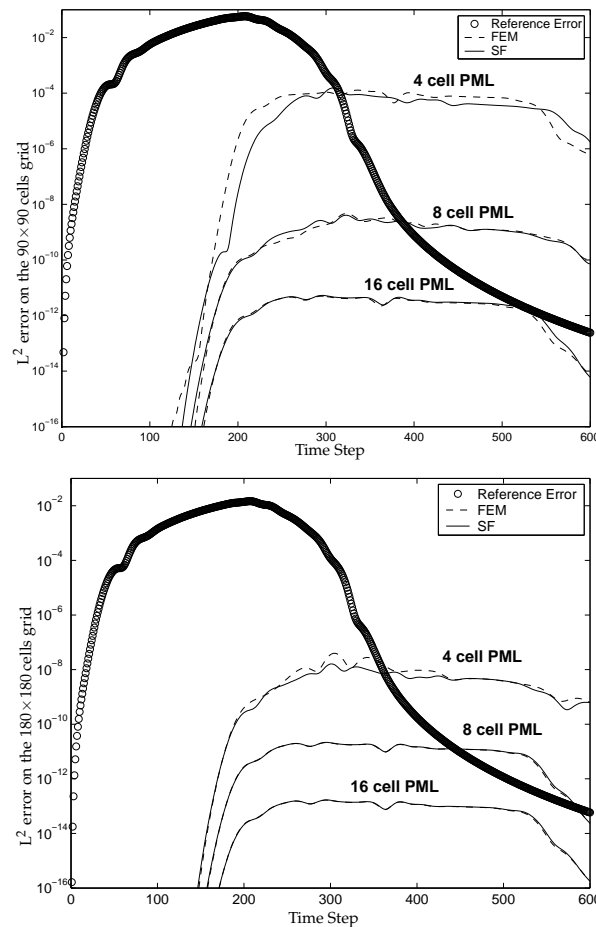


Figure 7: Comparison of the  $L^2$  error for the UPML with a mixed finite element scheme and the split field PML with the FDTD scheme on a  $90 \times 90$  cells grid (top) and for a  $180 \times 180$  cells grid (bottom). We note that as the grid is refined and/or as the number of PML cells is increased the error in the mixed FEM and FDTD schemes is about the same.

the above for three PML's containing 4, 8 and 16 cells. A comparison is presented with respect to the split field PML (SF) of Berenger discretized by the FDTD method, using the same test problem. The reference solution for the split-field case is constructed in a similar way. Fig. 7 shows the  $L^2$  error between the two reference solutions (Reference Error) for the FDTD and the mixed FEM, and the  $L^2$  error of the two schemes for 4, 8 and 16 cell PMLs each. From Fig. 7 (top), we can see that the reference error (discretization error) dominates for about 250 time steps. After this, as the wave exits the computational domain, the reflection error due to the PEC backed PML takes over. We have used 20 nodes/wavelength (i.e.,  $N=20$ ) in our calculations. As can be seen, for a 16 cell PML the reflection error is lower than the reference error. Fig. 7 (bottom) shows the  $L^2$  error between the two reference solutions (reference error) of the split-field and the mixed FEM,

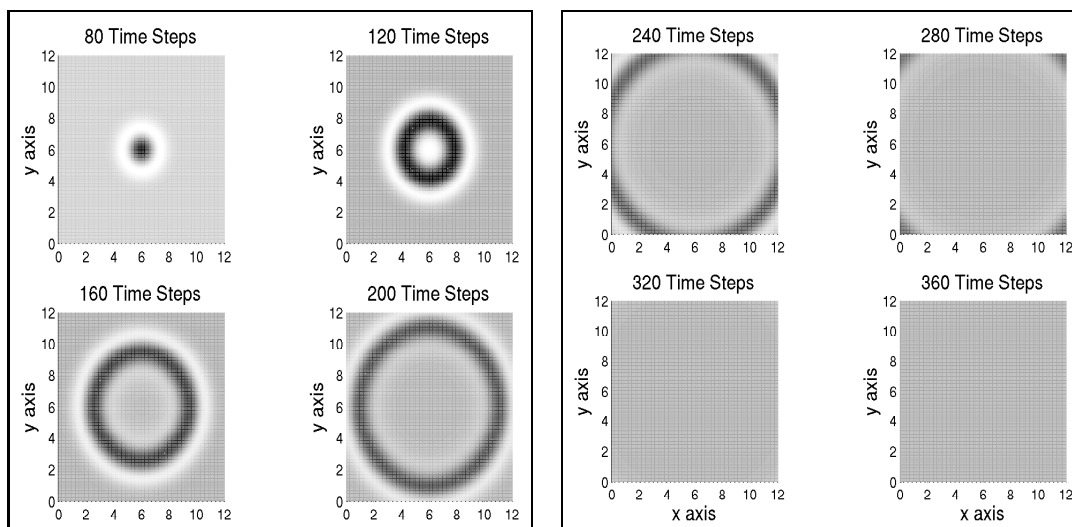


Figure 8: Propagation of the wave front. A top view of the solution is plotted at different time steps. The magnitude of the solution is the same for all time steps.

and the  $L^2$  error of the two schemes for 4, 8 and 16 cell PMLs, for a refined discretization. In this case,  $h = 1/15$  and  $\Delta t = 0.02/c$ . From Fig. 7 (bottom) we can see that a four cell PML provides a good absorbing layer.

In Fig. 8, we plot the propagation of a pulse on a  $180 \times 180$  cells domain backed by an eight cell PML obtained using the mixed FEM. The wave front completely disappears from the domain, as seen in the subplot corresponding to 320 time steps. All subplots are plotted at the same magnitude.

## 8 Conclusion

In this paper, we have presented and analyzed a mixed finite element scheme for the numerical solution of the 2D TM mode of the uniaxial PML. We have derived the numerical reflection coefficient for the UPML discretized by the mixed FEM and compared the results with the FDTD method. Based on our analysis, we can conclude that the proposed scheme has absorbing properties that are comparable to those of PML models discretized using FDTD. The extension of the mixed FEM to 3D is straightforward and uses a combination of Nédélec's elements and Nédélec-Raviart-Thomas elements for the discretization of the electric and magnetic fields, respectively.

As in the case of the FDTD method, we also find here that the choice of the PML conductivity affects the numerical reflection errors. Thus, a more rigorous analysis is needed to determine the optimal choice of the polynomial approximation to the PML conductivity that will minimize the numerical reflection errors that are generated using the mixed FEM.

## Acknowledgments

The authors would like to thank Dr. H. T. Banks, Dr. R. Glowinski, and Dr. Mac Hyman for fruitful discussions and for their tremendous support and encouragement. This work was supported in part by Los Alamos National Laboratory, an affirmative action/equal opportunity employer which is operated by the University of California for the United States Department of Energy under contract Nos W-7405-ENG-36, 03891-001-99-4G, 74837-001-03 49, and/or 86192-001-04 49, and in part by the U.S. Air Force Office of Scientific Research under grants AFOSR F49620-01-1-0026 and AFOSR FA9550-04-1-0220.

## References

- [1] S. Abarbanel and D. Gottlieb, A mathematical analysis of the PML method, *J. Comput. Phys.*, 134 (1997), 357-363.
- [2] S. Abarbanel, D. Gottlieb and J. S. Hesthaven, Well-posed perfectly matched layers for advective acoustics, *J. Comput. Phys.*, 154 (1999), 266-283.
- [3] A. Ahland, D. Schulz and E. Voges, Accurate mesh truncation for Schrödinger equations by a perfectly matched layer absorber: Application to the calculation of optical spectra, *Phys. Rev. B*, 60 (1999), 109-112.
- [4] J. P. Berenger, A perfectly matched layer for the absorption of electromagnetic waves, *J. Comput. Phys.*, 114 (1994), 185-200.
- [5] J. P. Berenger, Three dimensional perfectly matched layer for the absorption of electromagnetic waves, *J. Comput. Phys.*, 127 (1996), 363-379.
- [6] V. A. Bokil and M. W. Buksas, Comparison of a finite difference and a mixed finite element formulation of the uniaxial perfectly matched layer, Tech. Rep. CRSC-TR06-12, N. C. State University, February 2006.
- [7] V. A. Bokil and R. Glowinski, A distributed Lagrange multiplier based fictitious domain method for Maxwell's equations, *Int. J. Comput. Numer. Anal. Appl.*, 6 (2004), 203-245.
- [8] V. A. Bokil and R. Glowinski, An operator splitting scheme with a distributed Lagrange multiplier based fictitious domain method for wave propagation problems, *J. Comput. Phys.*, 205 (2005), 242-268.
- [9] W. C. Chew and W. H. Weedon, A 3D perfectly matched medium from modified Maxwell's equations with stretched coordinates, *Microw. Opt. Techn. Lett.*, 7 (1994), 599-604.
- [10] G. Cohen, P. Joly, J. Roberts and N. Tordjman, Higher order triangular finite elements with mass lumping for the wave equation, *SIAM J. Numer. Anal.*, 38 (2001), 2047-2078.
- [11] G. Cohen and P. Monk, Mur-Nédélec finite element schemes for Maxwell's equations, *Comput. Method. Appl. Mech. Engrg.*, 169 (1999), 197-217.
- [12] F. Collino and P. Monk, Optimizing the perfectly matched layer, *Comput. Method. Appl. Mech. Engrg.*, 164 (1998), 157-171.
- [13] R. Dautray and J.-L. Lions, *Mathematical Analysis and Numerical Methods for Science and Technology*, vol. 3, Springer-Verlag, Berlin Heidelberg, 1990.
- [14] S. D. Gedney, An anisotropic perfectly matched layer absorbing media for the truncation of FDTD lattices, *IEEE T. Antenn. Propag.*, 44 (1996), 1630-1639.
- [15] M. E. Hayder, F. Q. Hu and M. Y. Hussaini, Towards perfectly absorbing conditions for Euler equations, in: *AIAA 13th CFD Conference*, Paper 97-2075, 1997.

- [16] F. Q. Hu, On absorbing boundary conditions for linearized Euler equations by a perfectly matched layer, *J. Comput. Phys.*, 129 (1996), 201-219.
- [17] D. Johnson, C. Furse and A. Tripp, Application and optimization of the perfectly matched layer boundary condition for geophysical simulations, *Microw. Opt. Techn. Lett.*, 25 (2000), 254-255.
- [18] R. Mittra and U. Pikel, A new look at the perfectly matched layer (PML) concept for the reflectionless absorption of electromagnetic waves, *IEEE Microw. Guided Wave Lett.*, 5 (1995), 84-86.
- [19] M. Movahhedi, A. Abdipour, H. Ceric, A. Sheikholeslami and S. Selberherr, Optimization of the perfectly matched layer for the finite-element time-domain method, *IEEE Microw. Wirel. Components Lett.*, 17(1) (2007), 10-12.
- [20] C. M. Rappaport, Perfectly matched absorbing boundary conditions based on anisotropic lossy mapping of space, *IEEE Microw. Guided Wave Lett.*, 5 (1995), 90-92.
- [21] P. A. Raviart and J. M. Thomas, A mixed finite element method for 2nd order elliptic problems, in: I. Galligani and E. Magenes (Eds.), *Proc. of Math. Aspects on the Finite Element Method*, Lecture Notes in Mathematics, Springer-Verlag, vol. 606, 1977, pp. 292-315.
- [22] Z. S. Sacks, D. M. Kinsland, R. Lee and J. F. Lee, A perfectly matched anisotropic absorber for use as an absorbing boundary condition, *IEEE T. Antenn. Propag.*, 43 (1995), 1460-1463.
- [23] A. Taflove, *Advances in Computational Electrodynamics: The Finite-Difference Time-Domain Method*, Artech House, Norwood, MA, 1998.
- [24] J. We, D. Kinsland, J. Lee and R. Lee, A comparison of anisotropic PML to Berenger's PML and its application to the finite-element method of EM scattering, *IEEE T. Antenn. Propag.*, 45 (1997), 40-50.
- [25] J.-Y. Wu, J. Nehrbass and R. Lee, A comparison of PML for TVFEM and FDTD, *Int. J. Numer. Model.*, 13 (2000), 233-244.
- [26] K. S. Yee, Numerical solution of initial boundary value problems involving Maxwell's equations in isotropic media, *IEEE T. Antenn. Propag.*, 14 (1966), 302-307.
- [27] L. Zhao and A. Cangellaris, A general approach for the development of unsplit-field time-domain implementations of perfectly matched layers for FDTD grid truncation, *IEEE Microw. Guided Wave Lett.*, 6 (1996), 209-211.